Influence of symmetry on the second-order NLO properties

Beaujean, Pierre; Champagne, Benoît

Published in:
Pure and Applied Chemistry

DOI:
10.1515/pac-2025-0518

Publication date:
2025

Document Version
Publisher's PDF, also known as Version of record

Review Article

Pierre Beaujean and Benoît Champagne*

Influence of symmetry on the second-order NLO properties: insights from the few state approximations

https://doi.org/10.1515/pac-2025-0518
Received May 8, 2025; accepted July 3, 2025

Abstract: A series of valence bond charge-transfer (VB-*n*CT) models ($n \in [1, 4]$) are enacted to assess the influence of molecular symmetry on the second-order nonlinear optical (NLO) response, the first hyperpolarizability, β. This is accomplished for different amplitudes of the ground-state charge-transfer character, quantified by the VB-CT mixing parameter, m_{CT}. The analysis focuses on quantities accessible from the second harmonic scattering (SHS) phenomenon and measurements, β_{SHS} and its depolarization ratio. Among the symmetries considered, D_{3h} and C_{3v} (VB-3CT, with large θ, *i.e.* for almost planar tripod-shape molecules) yield the largest β_{SHS} values provided m_{CT} is large, followed by T_d (VB-4CT). These cases correspond to dominant octupolar responses and depolarization ratios close to 3/2. Other symmetries result in comparatively weaker responses, and a variety of depolarization ratios. Maximizing the charge-transfer dipole moment μ_{CT} and minimizing the ratio $\xi = T/t$, are also identified as critical factors for enhancing the second-order NLO responses.

Keywords: Few state models; first hyperpolarizability; molecular symmetry; nonlinear optics; quantum science and technology; second harmonic scattering.

Introduction

This paper focuses on the first hyperpolarizability, β, the molecular second-order nonlinear optical (NLO) response that is associated with phenomena like the second harmonic generation (SHG). Indeed, the discovery of Second Harmonic Generation (SHG) by Franken *et al.*[1] has fostered a large amount of research activities, aiming at applications in materials and life sciences. Applications encompass materials with large SHG responses for applications in frequency doublers[2] as well as the design of SHG sensors.[3–5] The SHG response is also probed to reveal the structure and dynamics of molecules[6,7] and interfaces.[8–10] Promising molecular architectures often belong to the push-pull family. These structures typically consist of a pair of electron donor and acceptor groups connected by a π-conjugated segment that facilitates the electronic "communication" between the two moieties.[11–14] To maximize β, two (non-orthogonal) strategies have been broadly employed: i) choosing an appropriate pair of donor and acceptor, and ii) controlling the length and nature of the π-conjugated path. To elucidate the relationships between the β response and the structure, simplified models have been developed to capture complex phenomena with minimal sets of parameters. The valence-bond charge-transfer (VB-CT) model,

Article note: A collection of invited papers to celebrate the UN's proclamation of 2025 as the International Year of Quantum Science and Technology.

***Corresponding author: Benoît Champagne**, Laboratory of Theoretical Chemistry, Unit of Theoretical and Structural Physical Chemistry, Namur Institute of Structured Matter, University of Namur, Rue de Bruxelles 61, B-5000 Namur, Belgium,
e-mail: benoit.champagne@unamur.be. https://orcid.org/0000-0003-3678-8875
Pierre Beaujean, Laboratory of Theoretical Chemistry, Unit of Theoretical and Structural Physical Chemistry, Namur Institute of Structured Matter, University of Namur, Rue de Bruxelles 61, B-5000 Namur, Belgium

pioneered by Mulliken,[15] has been particularly insightful in describing the first hyperpolarizabilities of push-pull polyenes. It also applies to other properties, such as UV/Vis absorption spectra and various physico-chemical characteristics.[16] This model represents a system as a superposition of two limiting states, a valence-bond state, ϕ_{VB}, and a charge-transfer state, ϕ_{CT}, related by the electron displacement from the donor to the acceptor (Fig. 1). Using fundamental parameters, such as the ionization energy of the donor, the electron affinity of the acceptor, and the coupling between these states, the VB-CT model provides valuable insight into structure-property relationships. Indeed, when combined with the sum-over-states (SOS) theory developed by Orr and Ward,[17] these models provide estimate of the β response and identification of valuable structure-property relationships.

Despite its simplicity, this model has proven versatile, allowing extensions to compounds with multiple donor/acceptor groups through 3-state,[18–20] 4-state,[21] and 5-state[22] descriptions. Further generalization are also possible[23] in order to get deeper understanding of the NLO responses, although at the cost of an increasingly large number of parameters. As shown in Fig. 2, the few state models are associated with chemical structures displaying various symmetries. However, to the best of our knowledge, while this approach has been extended to systems with larger n by others,[24] a comparative analysis of the NLO performances of these different compounds, supported by analytical expressions, has not yet been attempted. Therefore, this paper aims at enacting a comparative analysis of the VB-nCT models with n = 1–4 (Fig. 2). To provide further insights, this analysis is performed by analyzing β quantities that can be experimentally probed using the second harmonic scattering (SHS) technique.[25–29] It is organized as following: after a brief reminder of the different formulations of the VB-nCT models, of the relevant quantities, and of the different symmetries, the main results are compared. Finally, the last section draws conclusions and perspectives.

Theory

A model Hamiltonian for the VB-nCT model

Using the variational approach, given a set of basis functions $\{\phi_i\}$, the energy of a trial function $\Psi = \sum_i c_i\phi_i$ is always greater than or equal to the true ground state energy, $\mathcal{E}_0$:

$$\mathcal{E}_0 \leq \mathcal{E}, \text{ where } \mathcal{E} = \frac{\langle\Psi|H|\Psi\rangle}{\langle\Psi|\Psi\rangle}. \tag{1}$$

One minimizes the energy of the trial function by setting $\frac{d\mathcal{E}}{dc_i} = 0$. This yields a set of so-called secular equations of the form:

$$\forall k : \sum_i (H_{ki} - \varepsilon_k S_{ki})\, c_i = 0, \tag{2}$$

where $S_{ki} = \langle\phi_k|\phi_i\rangle$ (overlap matrix) and $H_{ki} = \langle\phi_k|\hat{H}|\phi_i\rangle$ (Hamiltonian matrix). This is a generalized eigenvalue problem. If the basis functions are orthogonal, *i.e.* $S_{ki} = \delta_{k,i}$, this reduces to a standard eigenvalue problem, $HC = C\varepsilon$, where diagonalizing H gives the energy levels, $\{\varepsilon_k\}$. C is the matrix of coefficients, also referred to as the eigenfunctions of the system.

In the VB-nCT framework, corresponding to a $(n+1)$-state model, a set of orthogonal functions is employed consisting of one valence-bond (VB) state, ϕ_{VB}, and n charge-transfer (CT) states, $\{\phi_{CT,i}|0 < i \leq n\}$. This leads to a model Hamiltonian, given by a $(n+1)\times(n+1)$ matrix and parameterized as follows:

$$\begin{aligned}
\langle\phi_{VB}|\hat{H}|\phi_{VB}\rangle &= E_{VB},\\
\langle\phi_{VB}|\hat{H}|\phi_{CT,i}\rangle &= -t,\\
\langle\phi_{CT,i}|\hat{H}|\phi_{CT,j}\rangle &= \begin{cases} E_{CT} & \text{if } i = j,\\ -T & \text{otherwise,}\end{cases}
\end{aligned} \tag{3}$$

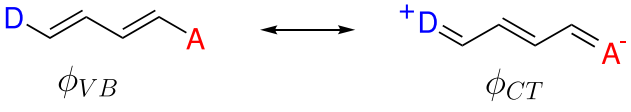

Fig. 1: Limiting forms of the VB-CT model.

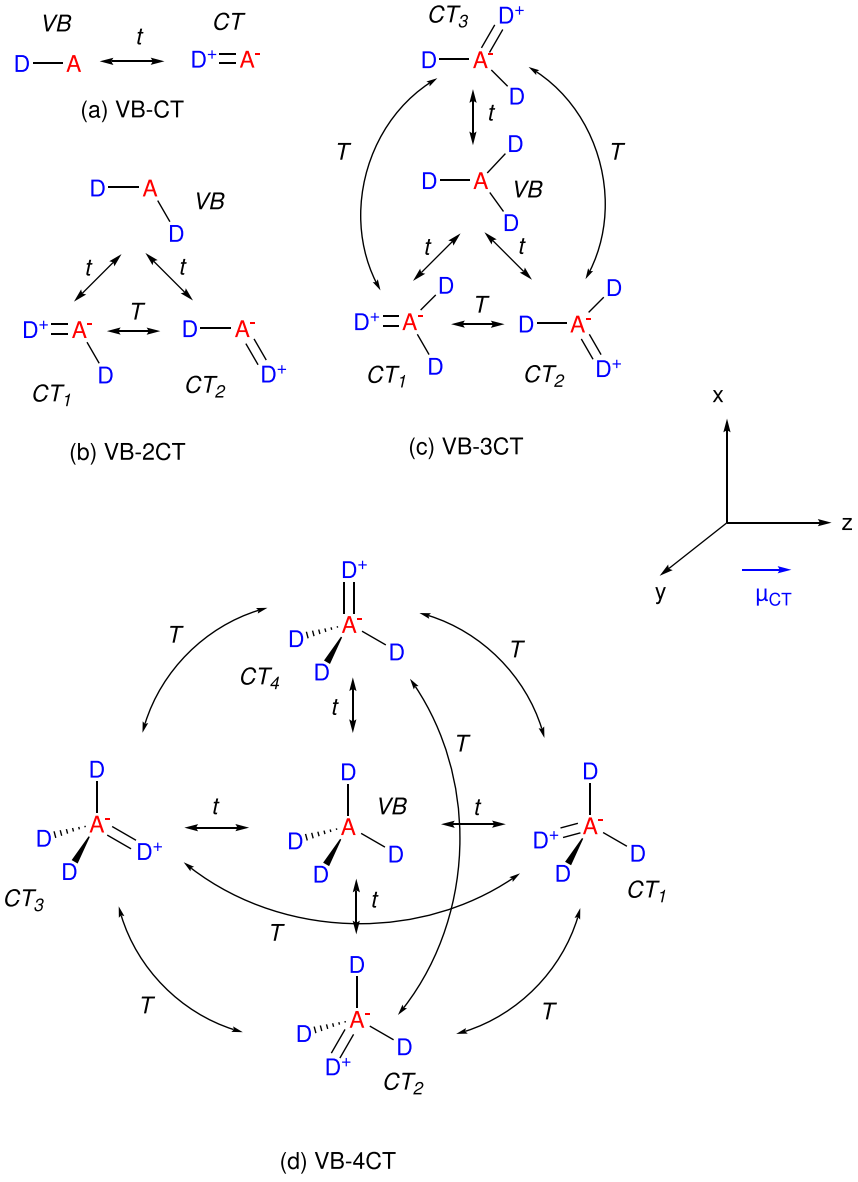

Fig. 2: Simplified representation of second-order NLO compounds displaying different symmetries and their successive VB-*n*CT models ($n \in [1, 4]$, adapted from Cho *et al.*,[22] with the charge transfer integrals t and T). Donor (D, in blue) and acceptor (A, in red) can be swapped without loss of generality.

where E_{VB} and E_{CT} denote the energies of the VB and CT states, respectively, while t and T are the transfer integrals.

Solving the eigenvalue problem yields a ground state, $|0\rangle$, with minimal energy, a set of $(n-1)$-fold degenerate excited states, $\{|e_i\rangle | 0 < i < n\}$ (which does not exist when $n = 1$), and a single non-degenerate excited state, $|f\rangle$. Corresponding eigenvalues were provided by Cho *et al.*[22] and are, in all generality, given by:

$$\begin{aligned} E_0 &= \frac{1}{2}\left[E_{VB} + E_{CT} - (n-1)T - \sqrt{(V-(n-1)T)^2 + 4nt^2}\right], \\ E_{e_i} &= E_{CT} + T, \\ E_f &= \frac{1}{2}\left[E_{VB} + E_{CT} - (n-1)T + \sqrt{(V-(n-1)T)^2 + 4nt^2}\right], \end{aligned} \tag{4}$$

where $V = E_{CT} - E_{VB}$. The associated eigenfunctions are:

$$\begin{aligned} |0\rangle &= \cos\delta\,|\phi_{VB}\rangle + \frac{\sin\delta}{\sqrt{n}}\sum_{0<j\le n}|\phi_{CT,j}\rangle, \\ |e_i\rangle &= \frac{1}{\sqrt{i(i+1)}}\left[-\sum_{0<j\le i}|\phi_{CT,j}\rangle + i|\phi_{CT,i+1}\rangle\right], \\ |f\rangle &= \sin\delta\,|\phi_{VB}\rangle - \frac{\cos\delta}{\sqrt{n}}\sum_{0<j\le n}|\phi_{CT,j}\rangle, \end{aligned} \tag{5}$$

where the mixing angle $\delta \in [0, \pi/2]$ is introduced. For $0 \le \delta < \pi/4$, the ground state is VB-dominated, whereas for $\pi/4 < \delta \le \pi/2$, the CT state dominates. The point $\delta = \pi/4$ is referred to as the *cyanine limit*.

Minimizing the ground-state energy E_0 with respect to δ (see eq. 1) provides a condition linking the parameters:

$$\frac{\partial E_0(\delta)}{\partial\delta} = 0 \Rightarrow V - (n-1)T = 2t\sqrt{n}\cot(2\delta). \tag{6}$$

Setting the energy origin to satisfy the following relationship:

$$E_{VB} + E_{CT} - (n-1)T = 0, \tag{7}$$

simplifies the eigenvalues to:

$$\begin{aligned} E_0 &= -\sqrt{n}\,\frac{t}{\sin(2\delta)}, \\ E_{e_i} &= nT + t\sqrt{n}\cot(2\delta), \\ E_f &= \frac{t}{\sin(2\delta)}\sqrt{n}. \end{aligned} \tag{8}$$

In the following analysis, difference between the state energies are employed:

$$\begin{aligned} \Delta E_{0e} &= E_{e_i} - E_0 = nT + t\sqrt{n}\cot(2\delta) + \sqrt{n}\,\frac{t}{\sin(2\delta)} = t\sqrt{n}\cot(\delta) + nT, \\ \Delta E_{0f} &= E_f - E_0 = \frac{2t\sqrt{n}}{\sin(2\delta)}. \end{aligned} \tag{9}$$

To monitor variations in molecular properties, the charge-transfer (CT) character of the ground state, ℓ_{CT}, can be introduced as follows:[20–22]

$$\ell_{CT} = \frac{1}{n}\sin^2\delta. \tag{10}$$

with $\delta \in [0, \pi/2]$, ℓ_{CT} varies in the range $\ell_{CT} \in [0, 1/n]$. A value of $\ell_{CT} = 0$ indicates a ground state fully described by the VB form, while $\ell_{CT} = 1/n$ corresponds to a state entirely characterized by CT. The eigenvalues become:

$$\begin{aligned} E_0 &= -\frac{t}{2\sqrt{\ell_{CT}\,(1-n\ell_{CT})}}, \\ E_{e_i} &= nT + \frac{t\,(1-2n\ell_{CT})}{2\sqrt{\ell_{CT}\,(1-n\ell_{CT})}} \\ E_f &= \frac{t}{2\sqrt{\ell_{CT}\,(1-n\ell_{CT})}}, \end{aligned} \tag{11}$$

and $|0\rangle$ and $|f\rangle$ may be also defined as ($|e_i\rangle$ remains the same):

$$\begin{aligned} |0\rangle &= \sqrt{1-n\ell_{CT}}\,|\psi_{VB}\rangle + \sqrt{\ell_{CT}}\sum_{j}^{n}|\psi_{CT,j}\rangle, \\ |f\rangle &= \sqrt{n\ell_{CT}}\,|\psi_{VB}\rangle - \sqrt{\frac{1}{n}-\ell_{CT}}\sum_{j}^{n}|\psi_{CT,j}\rangle, \end{aligned} \tag{12}$$

while the excitation energies become:

$$\Delta E_{0e} = nT + t\sqrt{\frac{1}{\ell_{CT}} - n}, \tag{13}$$

$$\Delta E_{0f} = \frac{t}{\sqrt{\ell_{CT}\,(1-n\ell_{CT})}}. \tag{14}$$

An additional parameter, introduced by Barzoukas and collaborators,[30–32] measures the VB-CT mixing:

$$m_{CT} = -\cos(2\delta) = 2n\ell_{CT} - 1. \tag{15}$$

This parameter, m_{CT}, ranges from –1 (VB-dominated) to +1 (CT-dominated), effectively capturing the balance between the VB and CT characters in the ground state. In that framework, the eigenvalues become:

$$\begin{aligned} E_0 &= -t\sqrt{\frac{n}{1-m_{CT}^2}}, \\ E_{e_i} &= nT - t\sqrt{n}\,\frac{m_{CT}}{\sqrt{1-m_{CT}^2}}, \\ E_f &= t\sqrt{\frac{n}{1-m_{CT}^2}}, \end{aligned} \tag{16}$$

and the excitation energies now read:

$$\begin{aligned} \Delta E_{0e} &= nT + t\sqrt{n\,\frac{1-m_{CT}}{1+m_{CT}}}, \\ \Delta E_{0f} &= 2t\sqrt{\frac{n}{1-m_{CT}^2}}. \end{aligned} \tag{17}$$

The evolution of excitation energies as a function of m_{CT} is shown in Fig. 3. Notably, both ΔE_{0e} and ΔE_{0f} diverge to $+\infty$ as $m_{CT} \to -1$. Similarly, ΔE_{0f} also tends to $+\infty$ when $m_{CT} \to 1$. Moreover, ΔE_{0e} exhibits a minimum at $m_{CT} = 1$, where $\Delta E_{0e} = nT$, while ΔE_{0f} reaches its minimum at $m_{CT} = 0$, with $\Delta E_{0f} = 2t\sqrt{n}$. Finally, decreasing both t and T leads to a decrease in ΔE_{0f} and ΔE_{0e}. This will become important in the following sections, since $X^{(n)} \propto \frac{1}{\Delta E^n} \propto \frac{1}{t^n}$ (see below).

Furthermore, $|0\rangle$ and $|f\rangle$ may be redefined, as:

$$\begin{aligned} |0\rangle &= \sqrt{\frac{1-m_{CT}}{2}}\,|\phi_{VB}\rangle + \sqrt{\frac{1+m_{CT}}{2n}}\sum_{j}^{n}|\phi_{CT,j}\rangle, \\ |f\rangle &= \sqrt{\frac{1+m_{CT}}{2}}\,|\phi_{VB}\rangle - \sqrt{\frac{1-m_{CT}}{2n}}\sum_{j}^{n}|\phi_{CT,j}\rangle. \end{aligned} \tag{18}$$

Sum-over-state (SOS) expression of NLO tensors

On the ground of perturbation theory, the SOS expression of Orr and Ward[17] states that, far from resonance, any component of any nonlinear optical tensor $X^{(n)}(-\omega_\sigma; \omega_1, \ldots)$ (of order n, so the polarizability, $\alpha = X^{(1)}$, the first hyperpolarizability $\beta = X^{(2)}$,or the second hyperpolarizability $\gamma = X^{(3)}$) is given by:

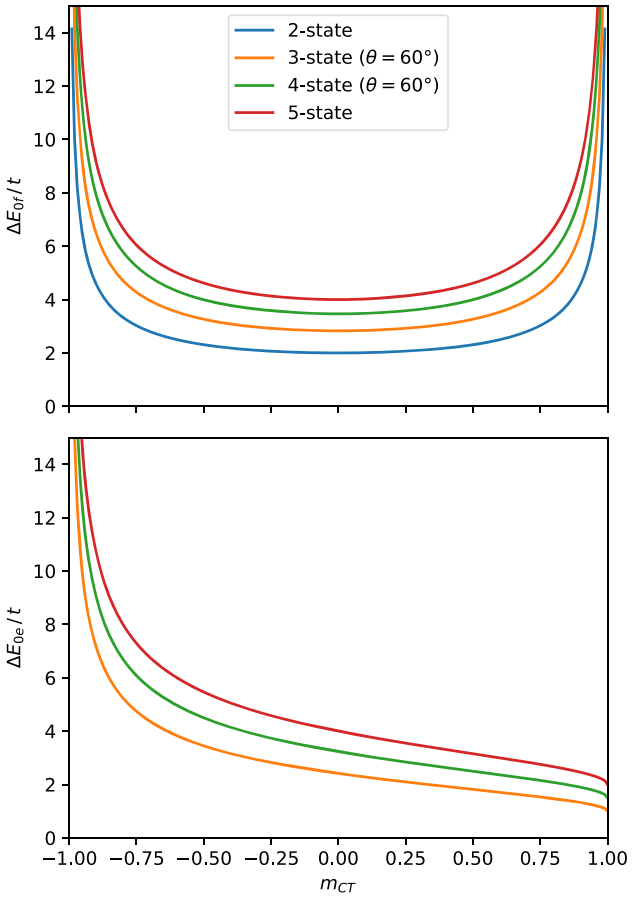

Fig. 3: Evolution of the reduced $|0\rangle \rightarrow |f\rangle$ ($\Delta E_{0f}/t$, unitless, top) and $|0\rangle \rightarrow |e\rangle$ ($\Delta E_{0e}/t$, unitless, bottom) excitation energies, computed using $T = t/2$, as a function of the charge transfer character of the ground state (m_{CT}). This figure, as well as the other graphs in this article, was generated using Matplotlib,[33] based on custom scripts implementing the analytical formulas.

$$X^{(n)}_{\zeta\eta\ldots\nu}(-\omega_\sigma\,;\omega_1,\ldots) = \hbar^{-n}\sum_{\mathcal{P}_F}\sum_{a_1,a_2\ldots\,a_n}\frac{\mu^{\zeta}_{0a_1}\mu^{\eta}_{a_1a_2}\cdots\mu^{\nu}_{a_n\,0}}{\prod\limits_{0<i\leq n}\left(\omega_{a_i}-\omega_\sigma+\sum\limits_{0<j<i}\omega_j\right)}, \tag{19}$$

where ζ, η, … are the Cartesian coordinates x, y, z (in the molecular frame), ω_1, ω_2…, the (optical) input frequencies of the laser for the NLO process (with $\omega_\sigma = \sum_{0<i\leq n}\omega_i$), $|a_1\rangle$, $|a_2\rangle$, …, the states of the system including the ground state (with $\hbar\omega_{a_i}$ the excitation energy from ground state to $|a_i\rangle$), $\mu^{\zeta}_{a_ia_j} = \langle a_i|\widehat{\zeta}|a_j\rangle$ the ζ component of the transition dipole moment from state a_i to a_j (it corresponds to the dipole moment of electronic state a_i when $i = j$), and $\sum_{\mathcal{P}_F}$ the sum of all permutations over each pair $(\zeta, -\omega_\sigma)$, (η, ω_1), …. However, this expression encounters divergences (or singularities) when a denominator vanishes. In the static case ($\forall i$: $\omega_i = 0$), it happens when the sum includes the ground state. Following Orr and Ward[17] and Bishop,[34] substituting the dipole operator in eq. 19 with a fluctuation dipole operator, $\bar{\mu}^{\zeta}_{a_1a_2} = \mu^{\zeta}_{a_1a_2} - \delta_{a_1a_2}\mu^{\zeta}_{00}$, allows the ground state to be excluded from the summations. Consequently, in the static case, one obtains the following expression for the β components:

$$\beta_{(\zeta\eta\kappa)} = \sum_{\mathcal{P}_F}\sum_{a_1',a_2'}\frac{(\zeta\bar{\eta}\kappa)_{a_1a_2}}{\Delta E_{0a_1}\,\Delta E_{0a_2}}, \tag{20}$$

where $\Delta E_{0a_1} = \hbar\omega_{a_1}$, and the prime indicates that the sums over a_j now exclude $|0\rangle$. Here, the simplified numerator notation of Bishop,[34] $(\zeta\eta\kappa)_{a_1a_2} = \mu^{\zeta}_{0a_1}\mu^{\eta}_{a_1a_2}\mu^{\kappa}_{a_20}$, is employed. Since this paper focuses on the static case, the permutation $\sum_{\mathcal{P}_F}$ runs over all components, so that $\beta_{\zeta\eta\kappa} = \beta_{\zeta\kappa\eta} = \beta_{\eta\zeta\kappa} = \ldots$, which is indicated using parentheses, $\beta_{(\zeta\eta\kappa)}$.

To utilize eq. 20, both excitation energies, calculated, in the VB-*n*CT model, as differences between eigenvalues, given in eq. 8 (or, in this contribution, eq. 17), and transition/excited-state dipoles are required. In general, these dipoles are computed as follows:

$$\vec{\mu}_{ij} = \langle i|\hat{\vec{\mu}}|j\rangle = \sum_{v\xi} C_{iv} C_{j\xi} \langle \phi_v|\hat{\vec{\mu}}|\phi_\xi\rangle = C_i M C_j^T, \tag{21}$$

where $|i\rangle = \sum_v C_{iv}|\phi_v\rangle$ represents the electronic states of the system, C_{iv} are the coefficients in the state expansion, and $|\phi_v\rangle$ are the basis functions. In the VB-*n*CT model, the dipole matrix elements $M_{v\xi} = \langle\phi_v|\hat{\mu}|\phi_\xi\rangle$ are approximated as follows:[35]

$$\begin{aligned} &\langle\phi_{VB}|\hat{\mu}|\phi_{VB}\rangle = \langle\phi_{VB}|\hat{\mu}|\phi_{CT,i}\rangle = 0, \\ &\langle\phi_{CT,i}|\hat{\mu}|\phi_{CT,j}\rangle = \begin{cases} \vec{\mu}_{CT,i} & \text{if } i = j, \\ 0 & \text{otherwise.} \end{cases} \end{aligned} \tag{22}$$

This results in a sparse, diagonal dipole matrix parameterized by a selected set of CT dipole moments associated to each CT state, $\{\vec{\mu}_{CT,i} \mid 0 < i \le n\}$. Generally, $\vec{\mu}_{CT,i} = \mu_{CT}\,\vec{e}_i$, where $\vec{e}_i$ is a unit vector, so that all dipole have the same length, given by the quantity μ_{CT}.

As a result, the ground-state, transition, and excited-state dipole moments are all proportional to μ_{CT}. Since the excitation energies scale with the parameter t (eq. 8), and in light of eq. 19, reduced hyperpolarizabilities (denoted with a tilde) are introduced in this work. These dimensionless quantities are defined for any component of the tensors, as:

$$\tilde{\beta} = \frac{\beta}{\mu_{CT}^3/t^2}. \tag{23}$$

Tensor invariants

For an isotropic medium composed of identical molecules or scatterers, the intensity, $I^{(n\omega)}$, of the incoherent contribution to the *n*-uple harmonic scattered light is proportional to an isotropic (or rotational) averaging of the tensor elements over all possible molecular orientations, $\langle X^{(n)}\rangle$.[25,36–38] For SHS, the conventional experimental setup is also referred to as the hyper-Rayleigh scattering (HRS) technique,[25] where the scattered light is analyzed at a 90° angle with respect to the direction of propagation (Y), the fundamental light beam (of frequency ω) is Z- or X-polarized (in the laboratory frame), while the Z-linearly polarized component of the scattered beam (of frequency 2ω) is recorded in the X direction. One can thus distinguish between two polarization combinations: the VV geometry (vertical-vertical, both incident and scattered lights are Z-polarized) and HV [horizontal-vertical, the incident (scattered) light is X (Z)-polarized]. The I_{VV} intensity is proportional to $\langle\beta_{ZZZ}^2\rangle$, while I_{HV} is proportional to $\langle\beta_{ZXX}^2\rangle$. For a non-polarized incident signal, both polarizations have equal probability and the intensity becomes proportional to the sum of the HV and VV observables. This allows defining β_{SHS}, the average first hyperpolarizability, and a depolarization ratio:

$$\beta_{SHS} = \sqrt{\langle\beta_{ZZZ}^2\rangle + \langle\beta_{ZXX}^2\rangle}, \tag{24}$$

$$\mathrm{DR}_{SHS} = \frac{\langle\beta_{ZZZ}^2\rangle}{\langle\beta_{ZXX}^2\rangle}. \tag{25}$$

Furthermore, the β tensor can be decomposed into irreducible spherical components.[39] When assuming the Kleinman's conditions (since only the static case is addressed in this article), β contains a dipolar ($J = 1$) and an octupolar ($J = 3$) component,[40] expressed as:

$$\left|\beta_{J=1}\right|^2 = \frac{3}{5}\sum_{\zeta\eta\kappa}^{x,y,z}\beta_{\zeta\eta\eta}\beta_{\zeta\kappa\kappa}, \left|\beta_{J=3}\right|^2 = \sum_{\zeta\eta\kappa}^{x,y,z}\beta^2_{\zeta\eta\kappa} - \frac{3}{5}\beta_{\zeta\eta\eta}\beta_{\zeta\kappa\kappa}. \tag{26}$$

As a consequence:

$$\begin{aligned}\langle\beta^2_{ZZZ}\rangle &= \frac{1}{5}\left|\beta_{J=1}\right|^2 + \frac{2}{35}\left|\beta_{J=3}\right|^2,\\ \langle\beta^2_{ZXX}\rangle &= \frac{1}{45}\left|\beta_{J=1}\right|^2 + \frac{4}{105}\left|\beta_{J=3}\right|^2.\end{aligned} \tag{27}$$

Notably, it implies that in the octupolar limit (when $|\beta_{J=3}|^2 \gg |\beta_{J=1}|^2$) $\mathrm{DR}_{SHS} \to \frac{3}{2}$, which is the minimal value it can take. It reaches a maximal value of 9 in the dipolar limit.[25]

Note that as a consequence of eq. 23, one can define $\tilde{\beta}_{SHS}$ in a similar way.

Model systems

The following model systems are considered in this article. For each of them, the expression for i) the ground-state, transition, and excited states dipole moments, ii) the non-null tensor components (obtained using eq. 19), and iii) the rotational invariants (obtained using eq. 27) are reported in the Supporting Information (SI).

Two-state $C_{\infty v}$ systems

This model consists of a single donor-acceptor (D/A) pair, typically positioned at the extremities of a π-conjugated linker. For convenience, it is oriented along the z-axis, such that the charge transfer dipole moment is given by:

$$\vec{\mu}_{CT} = \mu_{CT}\begin{pmatrix}0\\0\\1\end{pmatrix}.$$

Three-state C_{2v} systems

This system extends the two-state model by introducing two charge transfer (CT) states with dipole moments forming an angle $\theta \in [0, \pi/2]$ relative to the z-axis,[20] as illustrated in Fig. 4. The dipole moments are thus expressed as:

$$\vec{\mu}_{CT,1} = \mu_{CT}\begin{pmatrix}\sin\theta\\0\\\cos\theta\end{pmatrix}, \quad \vec{\mu}_{CT,2} = \mu_{CT}\begin{pmatrix}-\sin\theta\\0\\\cos\theta\end{pmatrix}.$$

In the limit $\theta \to \pi/2$, this model reduces to a $D_{\infty h}$ system, with a center of inversion, and a vanishing β response.

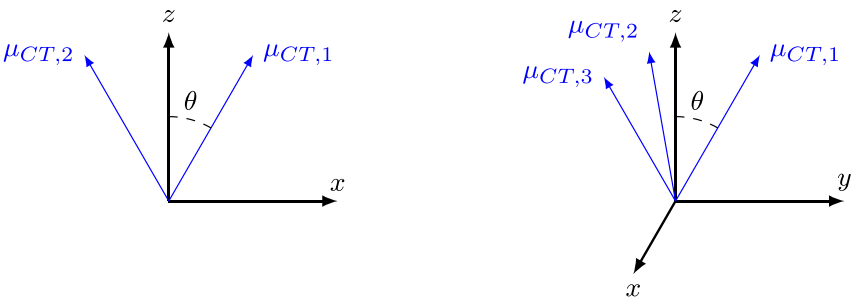

Fig. 4: Representation of the θ-dependent charge-transfer dipoles (μ_{CT}) in the 3-state (left) and 4-state (right) models.

Four-state C_{3v} system

This model consists of three charge transfer (CT) states arranged at 120° intervals in the xy-plane, with the first dipole aligned along the y-axis. Additionally, each dipole forms an angle $\theta \in [0, \pi/2]$ with the z-axis, as illustrated in Fig. 4. The dipole moments are therefore given by:

$$\vec{\mu}_{CT,1} = \mu_{CT} \begin{pmatrix} 0 \\ \sin\theta \\ \cos\theta \end{pmatrix}, \quad \vec{\mu}_{CT,2,3} = \mu_{CT} \begin{pmatrix} \pm\frac{\sqrt{3}}{2}\sin\theta \\ -\frac{1}{2}\sin\theta \\ \cos\theta \end{pmatrix}.$$

In the limit $\theta \to \pi/2$, this model reduces to a D_{3h} system.

Five-state T_d system

Finally, the T_d geometry is also considered.[22] In this contribution, the corresponding CT dipole moments are defined as:

$$\vec{\mu}_{CT,1} = \mu_{CT}\frac{\sqrt{3}}{3}\begin{pmatrix} 1 \\ 1 \\ 1 \end{pmatrix}, \quad \vec{\mu}_{CT,2} = \mu_{CT}\frac{\sqrt{3}}{3}\begin{pmatrix} 1 \\ -1 \\ -1 \end{pmatrix}, \quad \vec{\mu}_{CT,3} = \mu_{CT}\frac{\sqrt{3}}{3}\begin{pmatrix} -1 \\ -1 \\ 1 \end{pmatrix},$$

$$\vec{\mu}_{CT,4} = \mu_{CT}\frac{\sqrt{3}}{3}\begin{pmatrix} -1 \\ 1 \\ -1 \end{pmatrix}.$$

Results

Individual components

In this first part, a tensor component is assumed to follow the form:

$$\widetilde{\beta}_{\zeta\eta\kappa} \propto M(m_{CT}) \times E(m_{CT}, t, T) \times \Theta(\theta),$$

with the corresponding decomposition summarized in Table 1 (the full expressions are provided in the Supplementary Material). Certain components exhibit very similar expressions across different systems, leading to comparable m_{CT} dependencies. This is the case for β_{zzz} in the VB-nCT models for $n \in [1, 3]$, as well as β_{yyy} and $\beta_{(xyz)}$ for the VB-3CT and VB-4CT models, respectively.

Evolution of the response as a function of the symmetry

The evolution of the different invariants as a function of the symmetry of the system is then addressed in details. The evolution of $\widetilde{\beta}_{SHS}$ is shown in Fig. 5. To present the various results in a single graph, the values are plotted along a pathway illustrated in Fig. 6. This pathway represents a continuous transformation, starting from the VB-CT model and gradually adjusting the μ_{CT} values and θ angle to transition to the VB-4CT model.

Looking at Fig. 5, four main trends can be identified: (i) systems with non-equivalent μ_{CT}'s display smaller $\widetilde{\beta}_{SHS}$ than their fully-equivalent counterparts (except for $3s_1^* \to 3s_1$, due to the vanishing β response of the latter), (ii) positive and large values of m_{CT} are required to achieve high $\widetilde{\beta}_{SHS}$, (iii) highly symmetric systems

Table 1: Decomposition of the non-zero components into the functions that describe their behavior, for the different VB-nCT models ($n \in [1, 4]$).

	$M(m_{CT})$	$E(m_{CT}, t, T)$	$\Theta(\theta)$
	2-state $C_{\infty v}$		
$\tilde{\beta}_{zzz}$	$-m_{CT}\left(1-m_{CT}^2\right)$	ΔE_{0f}^{-2}	
	3-state $C_{2v} \rightarrow D_{\infty h}$		
$\tilde{\beta}_{zzz}$	$-m_{CT}\left(1-m_{CT}^2\right)$	ΔE_{0f}^{-2}	$\cos^3\theta$
$\tilde{\beta}_{(zxx)}$	$\left(1-m_{CT}^2\right)$	$2\,\Delta E_{0f}^{-1}\Delta E_{0e}^{-1} + \Delta E_{0e}^{-2}$	$\sin^2\theta\,\cos\theta$
	4-state $C_{3v} \rightarrow D_{3h}$		
$\tilde{\beta}_{zzz}$	$-m_{CT}\left(1-m_{CT}^2\right)$	ΔE_{0f}^{-2}	$\cos^3\theta$
$\tilde{\beta}_{(zyy)}$	$\left(1-m_{CT}^2\right)$	$2\,\Delta E_{0f}^{-1}\Delta E_{0e}^{-1} + \Delta E_{0e}^{-2}$	$\sin^2\theta\,\cos\theta$
$\tilde{\beta}_{yyy}$	$(1+m_{CT})$	ΔE_{0e}^{-2}	$\sin^3\theta$
	5-states T_d		
$\tilde{\beta}_{(xyz)}$	$(1+m_{CT})$	ΔE_{0e}^{-2}	

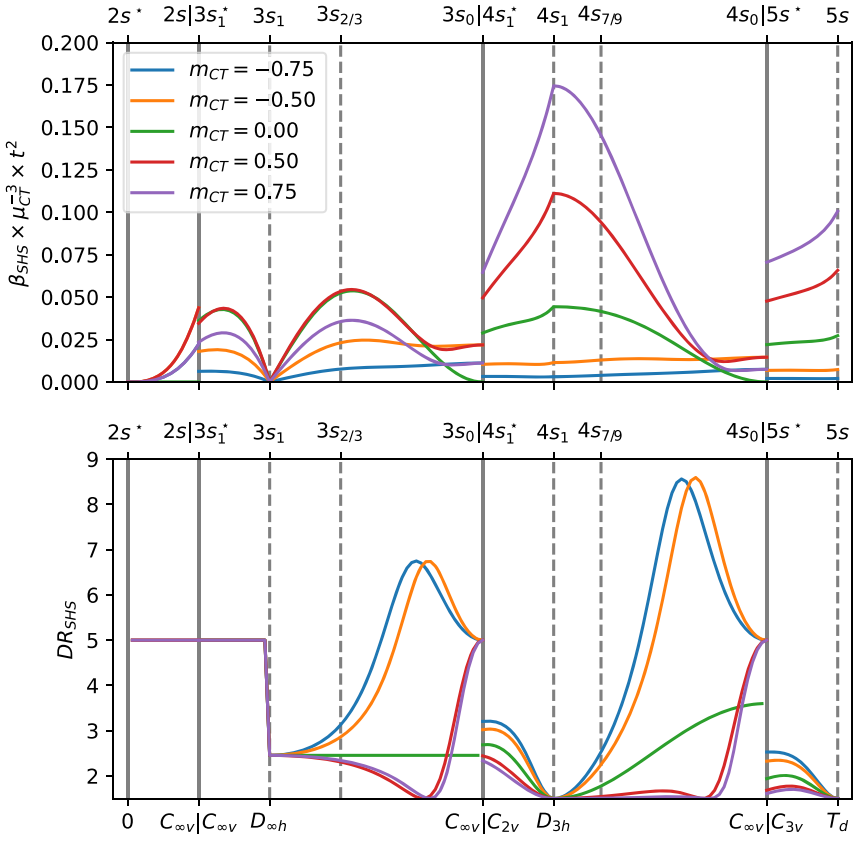

Fig. 5: Evolution of $\tilde{\beta}_{SHS}$ (top) and DR_{SHS} (bottom) as a function of the symmetry of the system and the charge transfer character of the ground state (m_{CT}), with $T = t/2$.

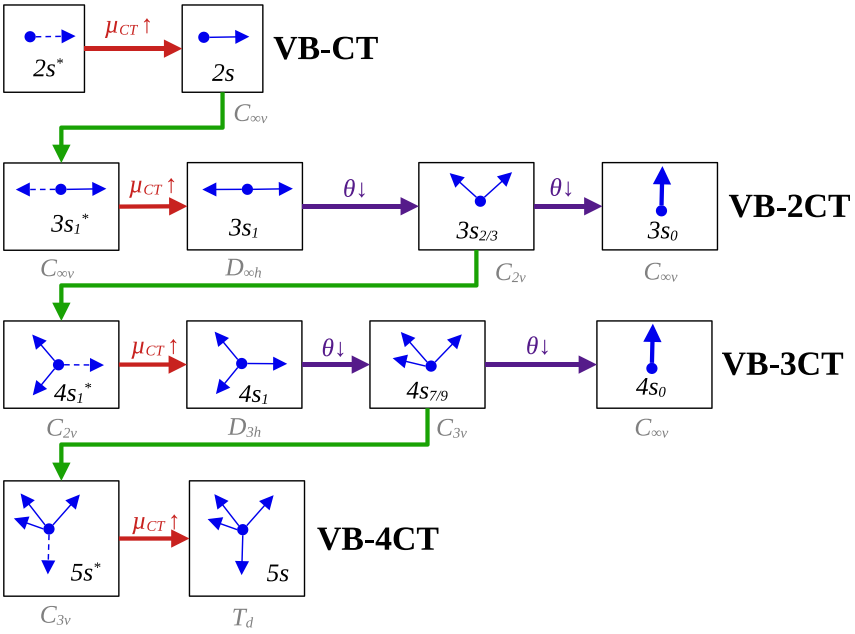

Fig. 6: Set of transformations for the 2-state to 5-state compounds explored in this article. The notation "ks" ($k \in [2, 5]$) represents a k-state system, corresponding to a VB-($k-1$)CT model (the CT dipoles, $\vec{\mu}_{CT}$, are indicated by blue arrows). The notation "ks^*" refers to a k-state model in which one of its μ_{CT} is given by $\vec{\mu}'_{CT} = \alpha\vec{\mu}_{CT}$ (indicated by a dashed line in the graph), which is gradually increased from $\alpha = 0$ (ks^*) to 1 (ks). Additionally, "ks_x" ($k = 3$, 4 and $x \in [0, 1]$) denotes a 3- or 4-state model with $\theta = \frac{x\pi}{2}$. Thus, a $ks^* \rightarrow ks$ symmetry transition corresponds to an increase in the initially missing μ_{CT}, leading to higher symmetry. Meanwhile, a $ks_1 \rightarrow ks_0$ transition corresponds to a decrease in θ, ultimately resulting in a $C_{\infty v}$ symmetry where all CT dipoles are parallel.

(D_{3h} and T_d) exhibit the largest $\tilde{\beta}_{SHS}$ values, and (iv) due to symmetry constraints, the values for C_{2v} at large θ and $D_{\infty h}$ are close to or exactly zero. Specifically, for $m_{CT} = 0.75$, the following ordering of responses is observed:

$$D_{3h} > C_{3v}\ (\text{large}\ \theta) > T_d > C_{2v}\ (\text{moderate}\ \theta) > C_{\infty v} \sim C_{2v}\ (\text{small}\ \theta) \sim C_{3v}\ (\text{small}\ \theta). \tag{28}$$

This trend persists at lower m_{CT} values, albeit with reduced values and differences between the symmetries. For $m_{CT} < -0.5$, the $\tilde{\beta}_{SHS}$ values tend to converge and become nearly indistinguishable across symmetries.

A decomposition into the dipolar and octupolar components (Fig. 7) provides further insight. On the one hand, large $\tilde{\beta}_{SHS}$ values are generally associated with dominant octupolar contributions (whose curves almost mirror the $\tilde{\beta}_{SHS}$ evolution), consistent with the findings of Zyss.[12] Such systems also exhibit small depolarization ratios (DR_{SHS}), approaching the octupolar limit of 3/2. On the other hand, systems with strong dipolar character, namely $C_{\infty v}$ and C_{2v} symmetries which correspond to the VB-CT and VB-2CT models, display significant $\tilde{\beta}_{SHS}$ values at moderate m_{CT}. This behavior is well-known in the context of the VB-CT model,[31] which reaches a maximum response at $m_{CT} = \pm\frac{\sqrt{5}}{5}$.

The behavior of the VB-2CT model is more complex to interpret, as it also depends on the angle θ. Two representative examples are shown in Fig. 8, which illustrate that the maximum of $\tilde{\beta}_{SHS}$ occurs at positive m_{CT} values and around $\theta \approx 54.9°$. This angle corresponds to the maximum of the function $\sin^2\theta\cos\theta$, which is located at $\theta = \tan^{-1}(\sqrt{2}) \approx 54.72°$. This observation suggests that, among the two nonzero and independent tensor components in this model [β_{zzz} and $\beta_{(zxx)}$, Table 1], $\beta_{(zxx)} \propto \sin^2\theta\cos\theta/(\Delta E_{ge}\,\Delta E_{gf})$ is the dominant one in this region. This is in agreement with the observation of Yang and his co-worker[20] for these systems. The influence of the parameter T is also evident: smaller T values yield larger $\tilde{\beta}_{SHS}$ amplitudes, with the peak shifting to higher m_{CT} values. This behavior is consistent with the inverse of the transition energies, since $\Delta E_{0e}^{-1}\,\Delta E_{0f}^{-1} \propto T^{-1}$. This evolution is further investigated below.

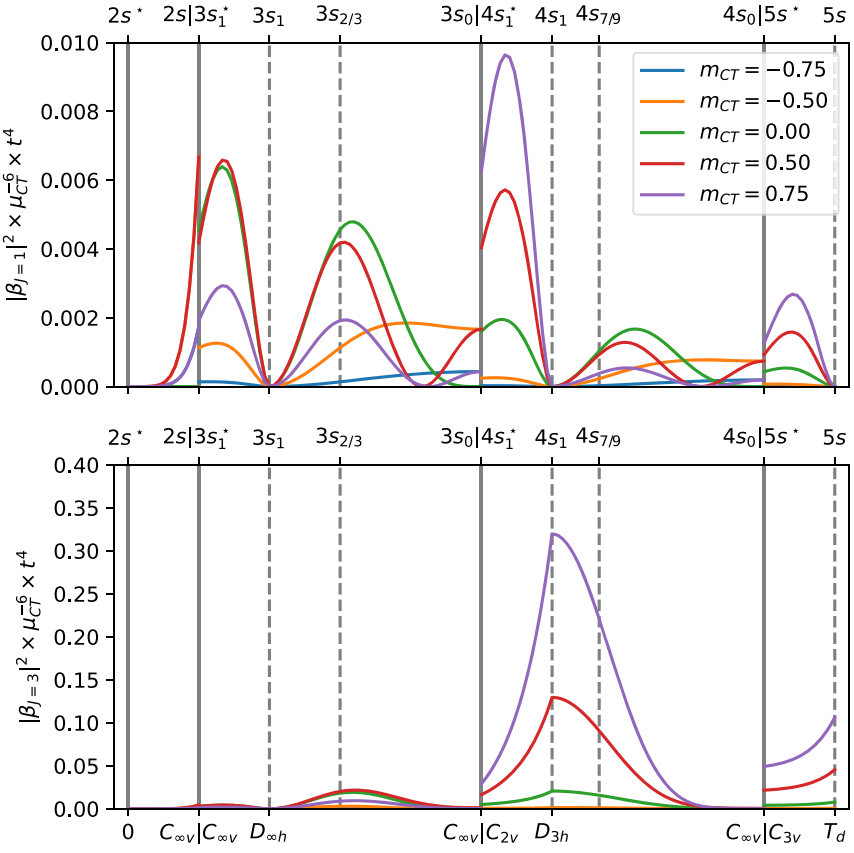

Fig. 7: Evolution of the reduced rotational invariants of the first hyperpolarizability tensor ($|\tilde{\beta}_{J=1}|^2$ and $|\tilde{\beta}_{J=3}|^2$, both unitless) as a function of the symmetry of the system and the charge transfer character of the ground state (m_{CT}), with $T = t/2$.

Further investigations on the systems with large β responses

As found in the previous section, the systems exhibiting the largest responses are the VB-3CT and VB-4CT models, particularly at $m_{CT} \to 1$ and $\theta \to 90°$ (corresponding to high symmetries). The corresponding approximate expressions for $\tilde{\beta}_{SHS}$ near $m_{CT} = 1$ are (notice that absolute values are used):

$$\tilde{\beta}_{SHS}[D_{3h}, m_{CT} = 1] = \frac{\sqrt{42}}{63\xi^2}\left|1 - \frac{2\sqrt{\frac{3}{2}(1 - m_{CT})}}{3T}\right|, \text{ and} \tag{29}$$

$$\tilde{\beta}_{SHS}[T_d, m_{CT} = 1] = \frac{\sqrt{21}}{84\xi^2}\left|1 - \frac{\sqrt{\frac{1}{2}(1 - m_{CT})}}{T}\right|, \tag{30}$$

which both display a depolarization ratio of $\frac{3}{2}$. Although these approximations quickly underestimate the values for $m_{CT} < 1$ (see Fig. 9), they satisfy the fact that the invariants reach their maxima at $m_{CT} = 1$, which could also help rationalize the ordering established in eq. 28. Moreover, these results indicate that achieving large responses requires minimizing T (and, to some extent, t).

To extend this analysis to the C_{3v} systems, one can examine the individual tensor components (reported in the Supplementary Material) near $\theta = 90°$, setting $m_{CT} = 1$. From Table 1, the only nonzero components is $\beta_{yyy} = -\beta_{(yxx)} \propto \sin^3\theta$, as illustrated in Fig. 10, where the approximate expressions from eq. 29, multiplied by the corresponding sine dependencies gives the θ evolution. This confirms that for this system, $\theta = 90°$ results in an extrema.

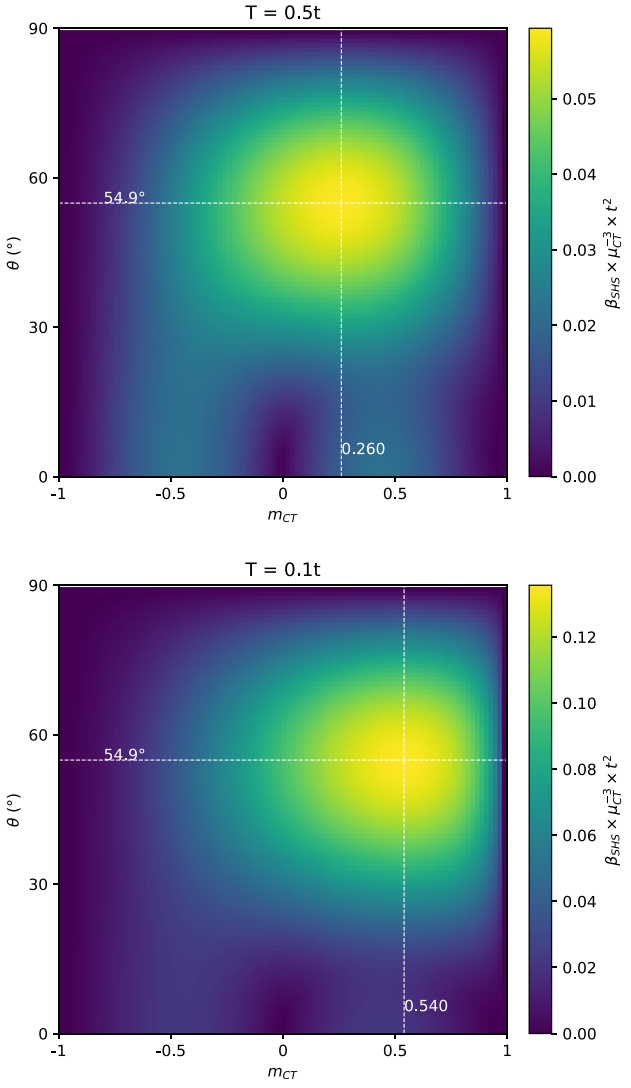

Fig. 8: Evolution of $\tilde{\beta}_{SHS}$ of the VB-2CT with m_{CT} and θ, with $T = t/2$ (top) and $T = t/10$ (bottom). Dashed line gives the approximate position of the maximum, found by taking the maxima in each heatmap.

Then, and since the seminal work of Oudar and Chemla[11] on the first hyperpolarizability, the VB-CT model has been instrumental in elucidating the structure–NLO activity relationship in materials.[30–32,35] As previously mentioned, the extrema are located at $m_{CT} = \pm\frac{\sqrt{5}}{5}$. Accordingly, the values of $\tilde{\beta}_{SHS}$ at these maxima amount to:

$$\tilde{\beta}_{SHS}[C_{\infty v}, m_{CT} = \pm\frac{\sqrt{5}}{5}] = \frac{6\sqrt{42}}{875} \tag{31}$$

It is associated with $\mathrm{DR}_{SHS} = 5$, which constitutes in both cases the so-called 1D limit.

Summarizing the observations so far, one gets, for a given value of $\xi = T/t$, the following relationships:

$$\tilde{\beta}_{SHS}[C_{3v}, m_{CT} = 1] \quad = \underbrace{\frac{4\sqrt{2}}{3}}_{\approx 1.89} \sin^3(\theta)\, \tilde{\beta}_{SHS}[T_d, m_{CT} = 1] = \underbrace{\frac{125}{54\xi^2}}_{\approx 2.32/\xi^2} \sin^3(\theta)\, \tilde{\beta}_{SHS}[C_{\infty v}, m_{CT} = \pm\frac{\sqrt{5}}{5}]. \tag{32}$$

This is one of the main results of this paper, which links the theoretical upper bonds of the SHS first hyperpolarizability invariants of compounds exhibiting different symmetries.

Finally, although it is not possible to derive an analytical expression for the maximum of β_{SHS} in the VB-2CT model,[20] it can be investigated numerically (Fig. 11). The results indicate that for small values of $\xi = T/t$, β_{SHS} reaches a maximum near $m_{CT} \approx 1$ and $\theta \approx 54.7°$, which corresponds to $\mathrm{DR}_{SHS} = 27/11 \approx 2.45$. This situation, when m_{CT}

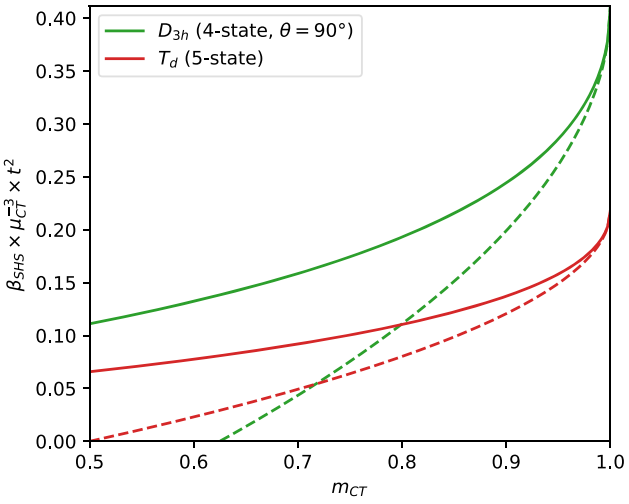

Fig. 9: Evolution of $\widetilde{\beta}_{SHS}$ for high-symmetry systems for $m_{CT} \to 1$, with $T = t/2$. Dashed line is an approximation obtained with a series around $m_{CT} = 1$ (eqs. 29 and 30).

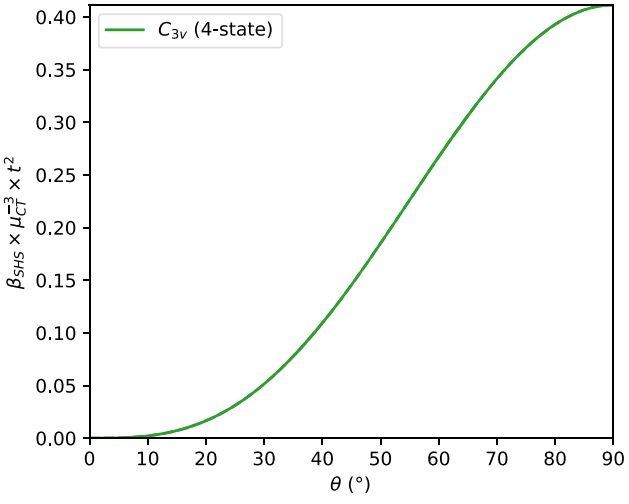

Fig. 10: Evolution of $\widetilde{\beta}_{SHS}$ of the VB-3CT model with θ at $m_{CT} = 1$, with $T = t/2$.

> 0, corresponds to a regime where $\beta_{(zxx)}$ dominates, particularly through its $\Delta E_{g\acute{e}}^{-2}$ contribution (Table 1). It should be noted that m_{CT} cannot be exactly equal to 1, as this would result in $\beta_{zzz} = \beta_{(zxx)} = 0$. Consequently, achieving large β_{SHS} values requires a delicate balance between maximizing m_{CT} and minimizing T. This numerical analysis nevertheless suggests that the values are, for ideal θ and m_{CT} values, larger than the maximum predicted for the $C_{\infty v}$ (VB-CT) symmetry (from eq. 31, $\widetilde{\beta}_{SHS} = 0.04$), and that the upper bound for $\widetilde{\beta}_{SHS}$ is approximately 0.225 for $m_{CT} \in (0.97, 0.98] \wedge \theta = \tan^{-1}(\sqrt{2}) \wedge \xi \leq 10^3$. However, in this case, the predicted first hyperpolarizability responses for the C_{3v} (VB-3CT) and T_d (VB-4CT) symmetries are orders of magnitude larger.

Further discussions, conclusions, and outlook

In this paper, VB-nCT models ($n \in [1, 4]$) have been investigated to assess the influence of symmetry and electronic structure parameters, particularly the ground-state charge-transfer character (quantified by the VB-CT mixing parameter, m_{CT}), on the second-order NLO responses. Special attention is given to quantities accessible from the second harmonic scattering technique, namely β_{SHS} and its corresponding depolarization ratio, which are determined by the first hyperpolarizability, β, tensor.

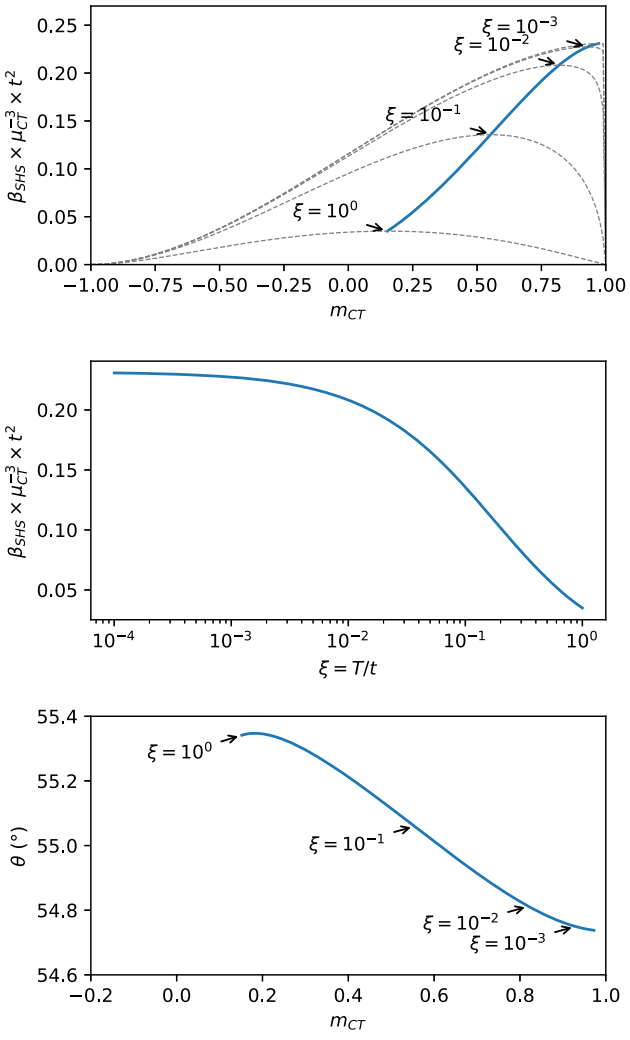

Fig. 11: Evolution of $\tilde{\beta}_{SHS}$ (top) and of its maximum (found numerically, blue curve in the top and middle panels), with $\xi = T/t$, for the VB-2CT model, and of the position of this maximum (bottom).

Symmetry considerations favor the C_{3v} symmetry (VB-3CT), which corresponds to tripod-like molecules, in particular those with large θ values (almost planar molecules) and its $\theta = 90°$ limiting case, which corresponds to a D_{3h} symmetry. The next best symmetry is the T_d case. These cases correspond to dominant octupolar responses and depolarization ratios close to 3/2. Other cases were explored, but they lead to smaller β_{SHS} values and a broader range of depolarization ratios. In all scenarios, ensuring a large μ_{CT} value and achieving a small ratio $\xi = T/t$ is critical for maximizing the NLO response, which, in practical terms, requires minimizing the first excitation energy ΔE_{ge}.

While feasible in principle, the different parameters (t, T, m_{CT}, μ_{CT}) are generally difficult to extract directly from experimental measurements, which makes difficult their use to infer and monitor these symmetry-property relationships. As a result, quantum chemistry calculations are of primary importance for the design of new compounds with enhanced NLO responses. Yet, among the experimental evaluations of these parameters, μ_{CT} can be inferred from UV/Vis absorption spectra. Then, estimating t or T can be achieved through projection methods, which involve partitioning the electronic Hamiltonian. A recent application of such approaches to intramolecular donor-acceptor systems can be found in the work of Gillet *et al.*,[41] following the methodology introduced by Baumeier *et al.*[26] More empirical models are also widely used: for example, the electron-in-a-box model, with its characteristic $\Delta E \propto L^{-2}$ dependence (where L is the box size), predicts that increasing the length of a π-conjugated segment (a common strategy to enhance NLO responses) leads to a decrease in t, up to a given point.[35] More generally, both t and T are dominated by electrostatic interactions at large intermolecular separations and

therefore decrease with distance. For T in particular, Förster theory approximates the interactions between CT states via dipole-dipole coupling, leading to $T \propto r^{-3}$, where r is the distance between dipoles.[28] Finally, m_{CT} (or equivalently ℓ_{CT}) has been linked to structural parameters such as the bond length alternation (BLA), as reported by Barzoukas *et al.*,[30,31] with a similarly strong correlation observed with the bond order alternation (BOA).[29]

In practice, achieving the ideal conditions explored in this study remains a significant challenge. One major difficulty is that real compounds are rarely perfectly symmetric and often possess multiple CT excited states of importance,[27] and both effects impact the NLO responses. Furthermore, obtaining large m_{CT} values requires a delicate balance between donor and acceptor strengths,[42,43] which is not easily achieved synthetically. However, quantum chemical calculations provide a valuable tool for exploring a wide chemical space and identifying promising candidates. While VB-CT models associated with quasi-one-dimensional compounds have been highly successful[13,44,45] and continue to drive the field forward,[14,29,46] octupolar systems are still comparatively less common, although the present work reaffirms their relevance. Hopefully, since the seminal contributions of Zyss,[12] a wide range of organic architectures have been explored, including C_{2v}-like[20,43,47] and octupolar systems,[6,21,48] offering numerous powerful design strategies. Beyond purely organic molecules, organometallic compounds consists of another efficient avenue, leveraging a variety of low-energy charge-transfer processes, such as metal-to-ligand charge transfer (MLCT). Among these, ruthenium- and iron-based complexes have been the most extensively studied,[49,50] though other metals have also been successfully incorporated into NLO-active materials.[51–53] Here, different ligands coordinated to the metal center enable fine-tuning of the electronic properties and facilitate access to a wide range of molecular symmetries.[7,42,50] Metal-organic frameworks (MOFs) also fall within this class of materials and, when carefully designed, can exhibit remarkable NLO properties.[54,55] It is expected that this work, combined with existing synthesis and measurement techniques, will contribute to the discovery of advanced molecules with large first hyperpolarizabilities, as well as materials exhibiting improved nonlinear optical susceptibilities.

Supplementary Material

For each VB-nCT model ($n \in [1, 4]$): i) the expression for all transition and excited state dipole moments, ii) the corresponding expression for all non-null tensor components, and iii) the expression of the tensor invariants.

Research ethics: Not applicable.
Informed consent: Not applicable.
Author contributions: All authors have accepted responsibility for the entire content of this manuscript and approved its submission.
Use of Large Language Models, AI and Machine Learning Tools: None declared.
Conflict of interest: The author states no conflict of interest.
Research funding: The authors acknowledge the F.R.S. – FNRS (Nonlinear chiroptics project) for the grants No. T.0025.22 and T.0052.24.
Data availability: The datasets generated and/or analyzed during the current study are available from the corresponding author on reasonable request.

References

1. Franken, P. A.; Hill, A. E.; Peters, C. W.; Weinreich, G. Generation of Optical Harmonics. *Phys. Rev. Lett.* **1961**, *7* (4), 118–119. https://doi.org/10.1103/physrevlett.7.118.
2. Konotop, V. V.; Kuzmiak, V. Nonreciprocal Frequency Doubler of Electromagnetic Waves Based on a Photonic Crystal. *Phys. Rev. B* **2002**, *66* (23), 235208. https://doi.org/10.1103/physrevb.66.235208.
3. Campagnola, P. J.; Wei, M.-D.; Lewis, A.; Loew, L. M. High-Resolution Nonlinear Optical Imaging of Live Cells by Second Harmonic Generation. *Biophys. J.* **1999**, *77* (6), 3341–3349. https://doi.org/10.1016/s0006-3495(99)77165-1.

4. Moreaux, L.; Sandre, O.; Blanchard-Desce, M.; Mertz, J. Membrane Imaging by Simultaneous Second-Harmonic Generation and Two-Photon Microscopy. *Opt. Lett.* **2000**, *25* (5), 320–322. https://doi.org/10.1364/ol.25.000320.
5. Tran, R. J.; Sly, K. L.; Conboy, J. C. Applications of Surface Second Harmonic Generation in Biological Sensing. *Annu. Rev. Anal. Chem.* **2017**, *10* (1), 387–414. https://doi.org/10.1146/annurev-anchem-071015-041453.
6. Beaujean, P.; Sanguinet, L.; Rodriguez, V.; Castet, F.; Champagne, B. Multi-State Second-Order Nonlinear Optical Switches Incorporating One to Three Benzazolo-Oxazolidine Units: A Quantum Chemistry Investigation. *Molecules* **2022**, *27* (9), 2770. https://doi.org/10.3390/molecules27092770.
7. Hood, B. R.; de Coene, Y.; Jones, C. F.; Lopez Poves, I.; Deveaux, N.; Halcovitch, N. R.; Champagne, B.; Clays, K.; Fielden, J. Synthesis and Optical and Nonlinear Optical Properties of Linear and Two-Dimensional Charge Transfer Chromophores Based on Polyoxometalates. *Inorg. Chem.* **2024**, *63* (51), 24250–24261. https://doi.org/10.1021/acs.inorgchem.4c04179.
8. Tonnelé, C.; Pielak, K.; Deviers, J.; Muccioli, L.; Champagne, B.; Castet, F. Nonlinear Optical Responses of Self-Assembled Monolayers Functionalized with Indolino–Oxazolidine Photoswitches. *Phys. Chem. Chem. Phys.* **2018**, *20* (33), 21590–21597. https://doi.org/10.1039/c8cp02991a.
9. Bouquiaux, C.; Tonnelé, C.; Castet, F.; Champagne, B. Second-Order Nonlinear Optical Properties of an Amphiphilic Dye Embedded in a Lipid Bilayer. A Combined Molecular Dynamics–Quantum Chemistry Study. *J. Phys. Chem. B* **2020**, *124* (11), 2101–2109. https://doi.org/10.1021/acs.jpcb.9b10988.
10. Ramos, T. N.; Champagne, B. Ramos and Benoît Champagne. Modeling Second Harmonic Generation at Alcohol/Air Interfaces. A Molecular Multi-Layer Approach. *J. Mol. Liq.* **2025**, *428*, 127499. https://doi.org/10.1016/j.molliq.2025.127499.
11. Oudar, J. L.; Chemla, D. S. Hyperpolarizabilities of the Nitroanilines and their Relations to the Excited State Dipole Moment. *J. Chem. Phys.* **1977**, *66* (6), 2664–2668. https://doi.org/10.1063/1.434213.
12. Zyss, J. Molecular Engineering Implications of Rotational Invariance in Quadratic Nonlinear Optics: From Dipolar to Octupolar Molecules and Materials. *J. Chem. Phys.* **1993**, *98* (9), 6583–6599. https://doi.org/10.1063/1.464802.
13. Bourhill, G.; Brédas, J.-L.; Cheng, L.-T.; Marder, S. R.; Meyers, F.; Perry, J. W.; Tiemann, B. G. Experimental Demonstration of the Dependence of the First Hyperpolarizability of Donor-Acceptor-Substituted Polyenes on the Ground-State Polarization and Bond Length Alternation. *J. Am. Chem. Soc.* **1994**, *116* (6), 2619–2620; https://doi.org/10.1021/ja00085a052.
14. Dalton, L. R.; Elder, D. L.; Johnson, L. E.; Robinson, B. H. 25 Years of Organic Electro-Optics and Future Prospects. *Nonlinear Opt. Quantum Opt.: Concepts Mod. Opt.* **2019**, *50* (1-3), 67–90.
15. Mulliken, R. S. Molecular Compounds and their Spectra. II. *J. Am. Chem. Soc.* **1952**, *74* (3), 811–824. https://doi.org/10.1021/ja01123a067.
16. Bender, C. J. Theoretical Models of Charge-Transfer Complexes. *Chem. Soc. Rev.* **1986**, *15* (4), 475. https://doi.org/10.1039/cs9861500475.
17. Orr, B. J.; Ward, J. F. Perturbation Theory of the Non-Linear Optical Polarization of an Isolated System. *Mol. Phys.* **1971**, *20* (3), 513–526. https://doi.org/10.1080/00268977100100481.
18. Hahn, S.; Kim, D.; Cho, M. Nonlinear Optical Properties of the Linear Quadrupolar Molecule: Structure-Function Relationship Based on a Three-State Model. *J. Phys. Chem. B* **1999**, *103* (39), 8221–8229. https://doi.org/10.1021/jp9836933.
19. Barzoukas, M.; Blanchard-Desce, M. Molecular Engineering of Push–Pull Dipolar and Quadrupolar Molecules for Two-Photon Absorption: A Multivalence-Bond States Approach. *J. Chem. Phys.* **2000**, *113* (10), 3951–3959. https://doi.org/10.1063/1.1288367.
20. Yang, M.; Champagne, B. Large Off-Diagonal Contribution to the Second-Order Optical Nonlinearities of Λ-Shaped Molecules. *J. Phys. Chem. A* **2003**, *107* (19), 3942–3951. https://doi.org/10.1021/jp0272567.
21. Cho, M.; Kim, H.-S.; Jeon, S.-J. An Elementary Description of Nonlinear Optical Properties of Octupolar Molecules: Four-State Model for Guanidinium-Type Molecules. *J. Chem. Phys.* **1998**, *108* (17), 7114–7120. https://doi.org/10.1063/1.476128.
22. Cho, M.; An, S.-Y.; Lee, H.; Ledoux, I.; Zyss, J. Nonlinear Optical Properties of Tetrahedral Donor–Acceptor Octupolar Molecules: Effective Five-State Model Approach. *J. Chem. Phys.* **2002**, *116* (21), 9165–9173. https://doi.org/10.1063/1.1473818.
23. Alam, M. M.; Beerepoot, M. T. P.; Ruud, K. A Generalized Few-State Model for the First Hyperpolarizability. *J. Chem. Phys.* **2020**, *152* (24), 244106. https://doi.org/10.1063/5.0010231.
24. Duboisset, J.; Brevet, P. F. Second-Harmonic Scattering-Defined Topological Classes for Nano-Objects. *J. Phys. Chem. C* **2019**, *123* (41), 25303–25308. https://doi.org/10.1021/acs.jpcc.9b04810.
25. Verbiest, T.; Clays, K.; Rodriguez, V. *Second-Order Nonlinear Optical Characterization Techniques: An Introduction*; Taylor & Francis: Boca Raton, 2009.
26. Baumeier, B.; Kirkpatrick, J.; Andrienko, D. Density-Functional Based Determination of Intermolecular Charge Transfer Properties for Large-Scale Morphologies. *Phys. Chem. Chem. Phys.* **2010**, *12* (36), 11103. https://doi.org/10.1039/c002337j.
27. Zhang, Y.; Castet, F.; Champagne, B. Theoretical Investigation of the First Hyperpolarizability Redox-Switching in a Ruthenium Complex. *Chem. Phys. Lett.* **2013**, *574*, 42–46. https://doi.org/10.1016/j.cplett.2013.04.071.
28. Sisto, A.; Glowacki, D. R.; Martinez, T. J. Ab Initio Nonadiabatic Dynamics of Multichromophore Complexes: A Scalable Graphical-Processing-Unit-Accelerated Exciton Framework. *Acc. Chem. Res.* **2014**, *47* (9), 2857–2866. https://doi.org/10.1021/ar500229p.
29. Dellai, A.; Naim, C.; Cerezo, J.; Prampolini, G.; Castet, F. Dynamic Effects on the Nonlinear Optical Properties of Donor Acceptor Stenhouse Adducts: Insights from Combined MD + QM Simulations. *Phys. Chem. Chem. Phys.* **2024**, *26* (18), 13639–13654. https://doi.org/10.1039/d4cp00310a.
30. Barzoukas, M.; Fort, A.; Blanchard-Desce, M. A Two-Form Description of Push-Pull Molecules: Correlations Between Structure, Intramolecular Charge Transfer and (Hyper)Polarizabilities. *J. Nonlinear Opt. Phys. Mater.* **1996**, *5* (4), 757–765. https://doi.org/10.1142/s0218863596000532.

31. Barzoukas, M.; Runser, C.; Fort, A.; Blanchard-Desce, M. A Two-State Description of (Hyper) Polarizabilities of Push-Pull Molecules Based on a Two-Form Model. *Chem. Phys. Lett.* **1996**, *257* (5–6), 531–537. https://doi.org/10.1016/0009-2614(96)00586-6.
32. Blanchard-Desce, M.; Barzoukas, M. Two-Form Two-State Analysis of Polarizabilities of Push Pull Molecules. *J. Opt. Soc. Am. B* **1998**, *15* (1), 302. https://doi.org/10.1364/josab.15.000302.
33. Hunter, J. D. Matplotlib: A 2d Graphics Environment. *Comput. Sci. Eng.* **2007**, *9* (3), 90–95. https://doi.org/10.1109/mcse.2007.55.
34. Bishop, D. M. Explicit Nondivergent Formulas for Atomic and Molecular Dynamic Hyperpolarizabilities. *J. Chem. Phys.* **1994**, *100* (9), 6535–6542. https://doi.org/10.1063/1.467062.
35. Lu, D.; Chen, G.; Perry, J. W.; Goddard, W. A. Valence-Bond Charge-Transfer Model for Nonlinear Optical Properties of Charge-Transfer Organic Molecules. *J. Am. Chem. Soc.* **1994**, *116* (23), 10679–10685. https://doi.org/10.1021/ja00102a037.
36. Andrews, D. L. Harmonic Generation in Free Molecules. *J. Phys. B* **1980**, *13* (20), 4091–4099. https://doi.org/10.1088/0022-3700/13/20/021.
37. Castet, F.; Bogdan, E.; Plaquet, A.; Ducasse, L.; Champagne, B.; Rodriguez, V. Reference Molecules for Nonlinear Optics: A Joint Experimental and Theoretical Investigation. *J. Chem. Phys.* **2012**, *136* (2), 024506. https://doi.org/10.1063/1.3675848.
38. Ford, J. S.; Andrews, D. L. Molecular Tensor Analysis of Third-Harmonic Scattering in Liquids. *J. Phys. Chem. A* **2018**, *122*, 563–573. https://doi.org/10.1021/acs.jpca.7b10333.
39. Jerphagnon, J.; Chemla, D.; Bonneville, R. The Description of the Physical Properties of Condensed Matter Using Irreducible Tensors. *Adv. Phys.* **1978**, *27* (4), 609–650. https://doi.org/10.1080/00018737800101454.
40. Brasselet, S.; Zyss, J. Multipolar Molecules and Multipolar Fields: Probing and Controlling the Tensorial Nature of Nonlinear Molecular Media. *J. Opt. Soc. Am. B* **1998**, *15* (1), 257. https://doi.org/10.1364/josab.15.000257.
41. Gillet, N.; Berstis, L.; Wu, X.; Gajdos, F.; Heck, A.; de la Lande, A.; Blumberger, J.; Elstner, M. Electronic Coupling Calculations for Bridge-Mediated Charge Transfer Using Constrained Density Functional Theory (CDFT) and Effective Hamiltonian Approaches at the Density Functional Theory (DFT) and Fragment-Orbital Density Functional Tight Binding (FODFTB) Level. *J. Chem. Theory Comput.* **2016**, *12* (10), 4793–4805. https://doi.org/10.1021/acs.jctc.6b00564.
42. Beaujean, P.; Champagne, B. Unraveling the Symmetry Effects on the Second-Order Nonlinear Optical Responses of Molecular Switches: The Case of Ruthenium Complexes. *Inorg. Chem.* **2022**, *61* (4), 1928–1940. https://doi.org/10.1021/acs.inorgchem.1c03077.
43. Postils, V.; Burešová, Z.; Casanova, D.; Champagne, B.; Bureš, F.; Rodriguez, V.; Castet, F. Second-Order Nonlinear Optical Properties of X-shaped Pyrazine Derivatives. *Phys. Chem. Chem. Phys.* **2024**, *26* (3), 1709–1721. https://doi.org/10.1039/d3cp04516a.
44. Dalton, L. R.; Gunter, P.; Jazbinsek, M.; Kwon, O.-P.; Sullivan, P. A. *Organic Electro-Optics and Photonics: Molecules, Polymers and Crystals*; Cambridge University Press: Cambridge, 2015.
45. Wu, J.; Li, Z.; Luo, J.; Jen, A. K.-Y. High-Performance Organic Second- and Third-Order Nonlinear Optical Materials for Ultrafast Information Processing. *J. Mater. Chem. C* **2020**, *8* (43), 15009–15026. https://doi.org/10.1039/d0tc03224g.
46. Dubuis, S.; Dellai, A.; Courdurié, C.; Owona, J.; Kalafatis, A.; Vellutini, L.; Genin, E.; Rodriguez, V.; Castet, F. Nonlinear Optical Responses of Photoswitchable Donor–Acceptor Stenhouse Adducts. *J. Am. Chem. Soc.* **2023**, *145* (19), 10861–10871. https://doi.org/10.1021/jacs.3c02778.
47. Castet, F.; Gillet, A.; Bureš, F.; Plaquet, A.; Rodriguez, V.; Champagne, B. Second-Order Nonlinear Optical Properties of Λ-Shaped Pyrazine Derivatives. *Dyes Pigm.* **2021**, *184*, 108850. https://doi.org/10.1016/j.dyepig.2020.108850.
48. Panja, N.; Ghanty, T. K.; Nandi, P. K. A Sum-Over-State Scheme of Analysis of Hyperpolarizabilities and its Application to Spiroconjugated Molecular System. *Theor. Chem. Acc.* **2010**, *126* (5), 323–337. https://doi.org/10.1007/s00214-009-0691-0.
49. Coe, B. J. Developing Iron and Ruthenium Complexes for Potential Nonlinear Optical Applications. *Coord. Chem. Rev.* **2013**, *257* (9–10), 1438–1458. https://doi.org/10.1016/j.ccr.2012.06.025.
50. Ashcroft, C. M.; Cole, J. M. 5 – Molecular Engineering of Organic and Organometallic Second-Order Nonlinear Optical Materials. In *Handbook of Organic Materials for Electronic and Photonic Devices (Second Edition)*, Woodhead Publishing Series in Electronic and Optical Materials; Ostroverkhova, O., Ed.; Woodhead Publishing: Cambridge, 2019; pp. 139–176.
51. Costes, J. P.; Lamère, J. F.; Lepetit, C.; Lacroix, P. G.; Dahan, F.; Nakatani, K. Synthesis, Crystal Structures, and Nonlinear Optical (NLO) Properties of New Schiff-Base Nickel(Ii) Complexes. Toward a New Type of Molecular Switch? *Inorg. Chem.* **2005**, *44*, 1973–1982. https://doi.org/10.1021/ic048578n.
52. Lamère, J. F.; Lacroix, P. G.; Farfán, N.; Rivera, J. M.; Santillan, R.; Nakatani, K. Synthesis, Characterization and Nonlinear Optical (NLO) Properties of a Push–Pull Bisboronate Chromophore with a Potential Electric Field Induced NLO Switch. *J. Mater. Chem.* **2006**, *16*, 2913–2920. https://doi.org/10.1039/b606359d.
53. Lacroix, P. G.; Malfant, I.; Lepetit, C. Second-Order Nonlinear Optics in Coordination Chemistry: An Open Door Towards Multi-Functional Materials and Molecular Switches. *Coord. Chem. Rev.* **2016**, *308*, 381–394. https://doi.org/10.1016/j.ccr.2015.05.015.
54. Medishetty, R.; Zaręba, J. K.; Mayer, D.; Samoć, M.; Fischer, R. A. Nonlinear Optical Properties, Upconversion and Lasing in Metal–Organic Frameworks. *Chem. Soc. Rev.* **2017**, *46*, 4976–5004. https://doi.org/10.1039/c7cs00162b.
55. Cheng, X.; Yao, J.; Zhang, H.; Wang, X.; Bai, J. The Nonlinear Optical Properties of Two-Dimensional Metal-Organic Framework. *J. Alloys Compd.* **2021**, *855*, 157433. https://doi.org/10.1016/j.jallcom.2020.157433.

Supplementary Material: This article contains supplementary material (https://doi.org/10.1515/pac-2025-0518).